Polymer 50 (2009) 5865–5870

Contents lists available at ScienceDirect

Polymer

journal homepage: www.elsevier.com/locate/polymer

Dynamics of monodisperse linear entangled polymer melts in extensional flow: The effect of excluded-volume interactions

Kalonji K. Kabanemi*, Jean-François Hétu

Industrial Materials Institute (IMI), National Research Council of Canada (NRC), 75 de Mortagne, Boucherville, Québec, Canada, J4B 6Y4

ARTICLE INFO

Article history:
Received 10 June 2009
Received in revised form
30 September 2009
Accepted 2 October 2009
Available online 9 October 2009

Keywords:
Extensional flow
Excluded-volume interactions
Polymer melts

ABSTRACT

We present an extension of the Rouse-CCR tube model for linear entangled polymers, by incorporating interchain repulsive excluded-volume interactions, to interpret extensional viscosity data of narrow molecular weight distribution polystyrene melts in strong extensional flows. The expression for the stress tensor is also adapted to account for modifications of the effective tube diameter due to flow-induced chain stretch. Despite its simplicity, the resulting model correctly captures the extensional rheological behavior of linear entangled monodisperse polystyrene melts already published in the literature.

1. Introduction

The dynamics of entangled polymer solutions and melts is strongly affected by the entanglements between polymer chains. The most successful theory that takes into account the effect of entanglements is based on the tube model [1–3]. The resulting standard tube-based models include the processes of reptation, convective constraint release (CCR), reptation-driven constraint release, chain stretch and contour length fluctuations (CLF). The physical picture underlying the tube model of polymer dynamics is that the motion of any chosen polymer chain is strongly restricted by the presence of surrounding polymers, which create a sort of a tube around the chosen chain. Such chains can interact strongly due to the topological constraints that chains cannot cross each other. The net effect of this is that the effective interchain interaction is repulsive. In atomistic and coarse-grained simulations [4,5], the interchain excluded-volume interactions ensure that different chains do not cut through each other, and contribute significantly to the stress when two chains try to cross each other. Such direct excluded-volume interactions were completely neglected in standard reptation-based theories. Recently, Marrucci and Iannirubertо [6,7] showed that data of extensional viscosity on monodisperse polystyrene melts by Bach et al. [8] cannot be interpreted within the available standard tube models [2,3,9]. Indeed, the data published by Bach et al. [8] and confirmed by Luap et al. [10] on monodisperse polystyrene melts show that the steady-state extensional viscosity decreases monotonically with the strain rate without any sign of an upturn at strain rate, $\dot{\varepsilon}$, of the order of the reciprocal Rouse time, τ_R, of the chain. In order to interpret the above mentioned extensional viscosity data, Marrucci and Iannirubertо [6,7] put forward the effects of the repulsive, interchain excluded-volume interactions among chain segments, which were neglected in standard tube theories for entangled polymers. They proposed a model for the dynamics of tube diameter, valid only in the range of strain rate smaller than the reciprocal Rouse time of the chain ($\dot{\varepsilon}\tau_R < 1$), that is based on the concept of thermal pressure exerted by the chain against the tube wall. In the flow range that has been considered ($\dot{\varepsilon}\tau_R < 1$), chain stretch occurs as a consequence of tube squeezing only. As a result, the stress was given by an average involving both tube orientation and tube diameter, as in the standard tube models. Therefore, this approach belongs to the category of decoupled approximation between tube orientation and tube diameter. We would like to emphasize that, in deriving their standard reptation-based model, Marrucci and Iannirubertо [3] recognized that the reason in the deficiencies in the tube model by Iannirubertо and Marrucci [11] is the decoupling approximation, which leads to the averages for the orientation tensor and the chain stretching. They pointed out that chain segments carry information on both orientation and stretching in a single quantity, that is the end-to-end vector $\boldsymbol{R}$, and care should be taken as to how to manipulate the averages based on this fundamental quantity. In this spirit, they proposed a simple model without decoupling approximation. In the same spirit, Likhtman and Graham [12] derived a simple single-mode equation, the Rouse-CCR tube model

* Corresponding author. Tel.: +1 450 641 5068; fax: +1 450 641 5106.
E-mail address: kalonji.kabanemi@cnrc-nrc.gc.ca (K.K. Kabanemi).

0032-3861/$ – see front matter
doi:10.1016/j.polymer.2009.10.008

for linear entangled polymers (Rolie-Poly equation), from a more complete molecular theory. Therefore, it seems to be worthwhile to build the analysis upon this simple molecular model, and then to incorporate all the ingredients necessary to describe the interchain excluded-volume interactions based on a molecular picture. This is the approach used in the present work, without decoupling approximation.

Wagner et al. [13] presented a generalized tube model with strain-dependent tube diameter, known as molecular stress function (MSF) theory. In MSF theory, tube stretch is caused by squeezing of the surrounding polymer chains, leading to a reduction of the tube diameter from its equilibrium value. The MSF model gives quantitative description of extensional flows. We would like also to point out that a tube-based model, with non-circular cross section, has been examined by Ianniruberto and Marrucci [14], but only with regard to the expression for the stress tensor, without considering the full dynamic evolution.

In this paper, we wish to extend the original Rolie-Poly model and to address the discrepancy between theoretical predictions and experimental data. Specifically, Bach et al. [8] and Luap et al. [10] showed that, in steady extensional flow the steady-state extensional viscosity of monodisperse linear entangled polystyrene melts decreases monotonically with the stain rate without any sign of upturn in the vicinity of $\dot{\varepsilon}\tau_R \approx 1$, and scales with $\dot{\varepsilon}^{-0.5}$ for large Deborah numbers. This discrepancy has been credited to the neglecting of direct interchain excluded-volume interactions. These interactions are included in the extended model by means of a repulsive interaction potential. Its behavior is analyzed in extensional flows and compared to experimental data of Bach et al. [8].

2. Rolie-Poly model with finite extensibility

In the original Rolie-Poly model [9,12], the conformation of the polymer chain, $\boldsymbol{\sigma}$, in a flow field, $\boldsymbol{u}$, evolves in time by an equation of the form

$$\dot{\boldsymbol{\sigma}} = \boldsymbol{L}\cdot\boldsymbol{\sigma} + \boldsymbol{\sigma}\cdot\boldsymbol{L}^T + \boldsymbol{f}(\boldsymbol{\sigma}), \tag{1}$$

where the tensor function, $\boldsymbol{f}$, is given by

$$\boldsymbol{f}(\boldsymbol{\sigma}) = -\frac{1}{\tau_d}(\boldsymbol{\sigma} - I) - \frac{2}{\tau_R}\left(1 - \sqrt{\frac{3}{tr\boldsymbol{\sigma}}}\right)\left(\boldsymbol{\sigma} + \beta\left(\frac{tr\boldsymbol{\sigma}}{3}\right)^{\delta}(\boldsymbol{\sigma} - I)\right). \tag{2}$$

Here $\boldsymbol{L} = \nabla\boldsymbol{u}^{\mathrm{T}}$ is the transpose of velocity gradient tensor, τ_d is the fixed-tube disengagement time or reptation time, τ_R is the longest Rouse time or stretch time, β is the CCR coefficient analogous to the coefficient introduced by Marrucci [15] in his original CCR paper, δ a negative power which can be obtained by fitting to the full theory, and $\boldsymbol{\sigma} = \boldsymbol{I}$ is the equilibrium value of the conformation tensor in the absence of flow.

We want to emphasize here that neither theory [9,12] has finite extensibility included, which would limit the degree of strain hardening in the stretching regime. Indeed, non-Gaussian behavior cannot be ignored in fast flows, when chains stretch significantly. In this spirit, Kabanemi and Hétu [16] derived a non-Gaussian version of the Rolie-Poly constitutive equation, which accounts for finite extensibility of polymer chains, by writing the tensor function, $\boldsymbol{f}$, in the following form

$$\boldsymbol{f}(\boldsymbol{\sigma}) = -\frac{1}{\tau_d}(\boldsymbol{\sigma} - I) - \frac{2}{\tau_R}k_s(\lambda)\left(1 - \sqrt{\frac{3}{tr\boldsymbol{\sigma}}}\right)\left(\boldsymbol{\sigma} + \beta\left(\frac{tr\boldsymbol{\sigma}}{3}\right)^{\delta}(\boldsymbol{\sigma} - I)\right), \tag{3}$$

where $k_s(\lambda)$ is the nonlinearity of the spring coefficient accounting for the finite extensibility of polymer chains, equals unity for linear springs and becomes much greater than unity as the spring becomes nearly fully stretched, and $\lambda = \sqrt{tr\boldsymbol{\sigma}/3}$ is the chain stretch ratio, and $\lambda = 1$ is its equilibrium value in the absence of flow.

In the limit of large stretch and in the absence of any other relaxation mechanisms, retraction, i.e., the trace of Eq. (1) with the expression for the tensor function, $\boldsymbol{f}$, given by Eq. (3), leads to the desired following relaxation for the stretch

$$\frac{d\lambda}{dt} = -\frac{1}{\tau_R}k_s(\lambda)(\lambda - 1). \tag{4}$$

This form was used in the MLD model with finite extensibility [17]. Note that in the limit of linear spring (Gaussian chain), $k_s(\lambda)$ remains unity, Eqs. (1) and (3) reduce to the original Rolie-Poly constitutive equation. The nonlinear spring coefficient, $k_s(\lambda)$, is approximated by the normalized Padé inverse Langevin function [17], i.e.,

$$k_s(\lambda) = \frac{\left(3 - \lambda^2/\lambda_{max}^2\right)\left(1 - 1/\lambda_{max}^2\right)}{\left(1 - \lambda^2/\lambda_{max}^2\right)\left(3 - 1/\lambda_{max}^2\right)}, \tag{5}$$

where λ_{max} is the maximum stretch ratio.

The constitutive equation, Eq. (1), with the expression for the tensor function, $\boldsymbol{f}$, given by Eq. (3) has to be completed by specifying the relationship between the polymeric stress contribution $\boldsymbol{\tau}_p$ and the conformation tensor $\boldsymbol{\sigma}$.

For this purpose, let us recall that, the physical picture of the tube model is that the motion of any chosen polymer chain is strongly restricted by the presence of surrounding polymer chains, which creates a sort of a tube around the chosen chain. The contour length of the tube is given by the primitive chain length, consisting of Z primitive path steps (subchains) which connect two consecutive entanglement points. At equilibrium, the average primitive path step or tube segment length, l_0, is expected to be of the same order as the equilibrium tube diameter a_0, and the equilibrium contour length of the whole tube is written as $L_0 = Z_0 l_0 = Z_0 a_0$, where Z_0 is the number of subchains (entanglements) per polymer chain at equilibrium. According to Gaussian chain statistics, $a_0 l_0 = N_{e0} b^2$ or $a_0^2 = N_{e0} b^2$, where b is the length of a "monomer" or a Kuhn segment, N_{e0} is the number of monomers between entanglements at equilibrium and $N = Z_0 N_{e0}$ is the number of monomers per polymer chain. The stretch of the tube segment, $\lambda = l/l_0$, is assumed to be uniform along the chain contour length, where l is the nonequilibrium tube segment length. Assuming that the number of monomers in each subchain does not change during flow, the entropic force in each subchain is given by

$$\boldsymbol{F}_{INTRA}(\boldsymbol{R}) = \frac{3k_BT}{N_{e0}b^2}k_s(\lambda)\boldsymbol{R} = \frac{3k_BT}{a_0^2}k_s(\lambda)\boldsymbol{R}, \tag{6}$$

where $\boldsymbol{R}$ is the end-to-end vector of the subchain, T the absolute temperature and k_B the Boltzmann constant. Assuming that the tube diameter stays constant and equal to its equilibrium value a_0, the polymeric stress contribution due to traction along the tube axis, $\boldsymbol{\tau}_p^{INTRA}$, is written as

$$\boldsymbol{\tau}_p^{INTRA} = cZ_0\langle\boldsymbol{F}_{INTRA}\boldsymbol{R}\rangle, \tag{7}$$

or by making use of Eq. (6), we can write Eq. (7) as

$$\boldsymbol{\tau}_p^{INTRA} = cZ_0 3k_BTk_s(\lambda)\frac{\langle\boldsymbol{RR}\rangle}{a_0^2} = cN3k_BT\frac{b^2}{a_0^2}k_s(\lambda)\frac{\langle\boldsymbol{RR}\rangle}{a_0^2}. \tag{8}$$

Here the factor cZ_0, accounts for the number of subchains (entanglements) at equilibrium per unit volume, c is the number of

polymer chains per volume and the factor cN, accounts for the number of monomers per unit volume. In terms of the conformation tensor, $\boldsymbol{\sigma}$, Eq. (8) can be written as

$$\boldsymbol{\tau}_p^{INTRA} = Gk_s(\lambda)(\boldsymbol{\sigma}-\mathbf{I}) = \frac{\eta_0}{\tau_d}k_s(\lambda)(\boldsymbol{\sigma}-\mathbf{I}), \tag{9}$$

where $G = cZ_0 3k_BT = cN3k_BT\frac{b^2}{a_0^2}$ is the plateau modulus, and η_0 is the zero- shear-rate polymer viscosity. This equation ensures that at equilibrium the polymer stress is zero.

3. Model with a variable tube diameter

The physics that is still missing from the above model, Eqs. (1), (3) and (9), is the deformation of the confining tube diameter itself. It is very natural to assume that the diameter of the confining tube changes upon deformations, as chains move closer together or further apart. Because the tube corresponds to topological constraints created by its surrounding, Marrucci and Cindo [18] introduced segmental stretch, where all rheological properties are assumed to be dominated by intramolecular forces, assuming that the tube deforms affinely with macroscopic strain. They assumed that whenever a subchain changes its length, the diameter of the tube that surrounds the subchain changes, so as to keep the volume of the tube segment constant (incompressibility assumption). Since on the average the subchain length increases, the tube diameter correspondingly decreases. We assume that the tube segment keeps a circular cross section shape even under high deformation. The effective diameter of the deformed tube, a, should shrink by a factor, $\sqrt{\lambda}$. Thus, the primitive chain should experience topological constraints at an average distance of

$$a = \frac{a_0}{\sqrt{\lambda}}. \tag{10}$$

Therefore, the tube diameter reduction arises as a consequence of the tube stretch, whose dynamics is described by Eqs. (1), (3) and (9). In rapidly changing flows, when chains stretch significantly, $\lambda = l/l_0 > 1$. The average primitive path step or tube segment length, l, is no longer of the same order as the equilibrium tube diameter a_0 or the current tube diameter a. It follows that under nonequilibrium conditions, $al = N_e b^2 = a_0^2\sqrt{\lambda}$, where N_e is the effective number of monomers between entanglements. Thus the effective number of monomers between entanglements during flow is increased from N_{e0} to $N_e = N_{e0}\sqrt{\lambda}$ and the number of subchains is reduced from Z_0 to $Z = N/N_e = Z_0/\sqrt{\lambda}$. Thus the entropic force in each subchain, defined by Eq. (6), can be rewritten as

$$\boldsymbol{F}_{INTRA}(\boldsymbol{R}) = \frac{3k_BT}{N_e b^2}k_s(\lambda)\boldsymbol{R} = \frac{3k_BT}{N_{e0}b^2}k_s(\lambda)\frac{1}{\sqrt{\lambda}}\boldsymbol{R} = \frac{3k_BT}{a_0^2}k_s(\lambda)\frac{1}{\sqrt{\lambda}}\boldsymbol{R}. \tag{11}$$

Unlike the entropic force derived by Marrucci and Cindo [18], Eq. (11) accounts for finite extensibility of the chain. Therefore, the polymeric stress contribution, $\boldsymbol{\tau}_p^{INTRA}$, is written as

$$\boldsymbol{\tau}_p^{INTRA} = cZ\langle \boldsymbol{F}_{INTRA}\boldsymbol{R}\rangle = cZ_0 3k_BTk_s(\lambda)\frac{1}{\lambda}\frac{\langle \boldsymbol{RR}\rangle}{a_0^2}, \tag{12}$$

or

$$\boldsymbol{\tau}_p^{INTRA} = Gk_s(\lambda)\frac{1}{\lambda}(\boldsymbol{\sigma}-I) = \frac{\eta_0}{\tau_d}k_s(\lambda)\frac{1}{\lambda}(\boldsymbol{\sigma}-I). \tag{13}$$

The difference between Eq. (13) and Eq. (9), which does not include the deformation of the tube diameter, is the pre-factor, $1/\lambda$, which now appears in Eq. (13). This expression for the stress tensor only accounts for intrachain forces, i.e., traction along the tube segment axis. It also accounts for the tube diameter reduction, in terms of the stretch ratio, λ, through the relation, $a = a_0/\lambda$. The contribution to the stress arising from the direct interaction with the surrounding chains which create a tube around the chosen chain is still neglected in the model.

We now need to account for the pressure that the confined chain exerts on its tube of constraints, i.e., the direct interchain excluded-volume interactions. As described above, in the stretching regime ($\dot{\varepsilon}\tau_R > 1$) under nonequilibrium conditions, the primitive chain experiences topological constraints at an average distance, $a = a_0/\lambda$, smaller than the equilibrium distance, a_0. The interaction between the test chain and the topological constraints generates repulsive force acting on the beads of the chain. In order to include the interchain, repulsive excluded-volume interactions, the entanglement effect is assumed to be repulsive interaction between the polymer chain in the tube and the entanglement points (the obstacles). This is done by means of a repulsive potential due to the topological interactions. The repulsive interchain interactions are accounted for through a shifted, truncated Lennard-Jones potential (LJ potential) acting on the chain beads [19]. The LJ potential is given by

$$U_{LJ}(r) = \begin{cases} \frac{k_BT}{2}\left[\left(\frac{a_{LJ}}{r}\right)^{12} - \left(\frac{a_{LJ}}{r}\right)^{6} + \frac{1}{4}\right], & r \le 2^{1/6}a_{LJ} \\ 0, & r < 2^{1/6}a_{LJ} \end{cases}, \tag{14}$$

and the corresponding force law obtained from this potential is

$$\boldsymbol{F}_{LJ}(\boldsymbol{r}) = -\frac{3k_BT}{a_{LJ}^2}\left[-2\left(\frac{a_{LJ}}{r}\right)^{14} + \left(\frac{a_{LJ}}{r}\right)^{8}\right]\boldsymbol{r}, \quad r \le 2^{1/6}a_{LJ}, \tag{15}$$

where $\boldsymbol{r}$ is the radial vector of the circular cross section of the tube segment, $r = |\boldsymbol{r}| = a$, and a_{LJ} is the distance at which the potential is zero. Inspired by Ianniruberto and Marrucci [14], we reinterpret this force as due to a "virtual spring" which connects the bead in the radial direction to the cylindrical surface of the tube of constraints, i.e. the force pushing against the wall of the tube segment. By setting a_{LJ}, the Lennard–Jones length to the equilibrium tube diameter, $a_{LJ} = a_0$ (length scales comparable to the equilibrium tube diameter), it can be shown that

$$\boldsymbol{F}_{LJ}(\boldsymbol{r}) = \frac{3k_BT}{a_0^2}\left(2\lambda^7 - \lambda^4\right)\boldsymbol{r} = \frac{3k_BT}{a_0^2}k_{LJ}(\lambda)\boldsymbol{r}. \tag{16}$$

We emphasize that, the Lennard–Jones length could be, as well, set to a value smaller than the equilibrium tube diameter a_0, which would reduce the length scale of the repulsive potential. The coefficient $k_{LJ}(\lambda) = (2\lambda^7 - \lambda^4)$ in Eq. (16) is the nonlinear coefficient of the "virtual spring" that is written here in terms of the stretch ratio, λ, instead of the tube diameter itself. At equilibrium, $\lambda = 1$, and therefore $k_{LJ} = 1$. Thus, it is easily found from Eq. (16) that the equilibrium force of the "virtual spring" becomes

$$F_{LJ} = \frac{3k_BT}{a_0}. \tag{17}$$

During deformation under nonequilibrium conditions, the effective diameter of the deformed tube, a, should shrink by a factor of $\sqrt{\lambda}$. Thus, the magnitude of the repulsive force pushing against the wall of the tube, Eq. (16), is

$$F_{LJ} = \frac{3k_BT}{a_0^2}k_{LJ}(\lambda)a = \frac{3k_BT}{a_0^2}k_{LJ}(\lambda)\frac{a_0}{\sqrt{\lambda}}. \tag{18}$$

We assume that the repulsive force, which acts against the tube wall, remains uniform along the axial direction. From constant

cylindrical tube volume arguments, a uniform radial repulsive force on the wall of the tube becomes equivalent to traction along the tube segment axis. Thus, the radial repulsive force also causes an increasing of tension in the axial direction. Such a method has also been used by Ianniruberto and Marrucci [14] who derived the expression of the stress tensor for tubes with circular cross section by using explicitly a confining potential. They demonstrated that, due to the axial symmetry of the circular tube, the contribution arising from the pressure on the wall of the confining cylindrical tube effectively corresponds to traction alongside the tube axis. Hence, by making use of the unit vector $\boldsymbol{R}/R$, the corresponding force along the tube axis can be written as

$$\mathbf{F}_{\mathrm{LJ}}(\boldsymbol{R}) = \frac{3k_{\mathrm{B}}T}{a_0^2}k_{\mathrm{LJ}}(\lambda)\frac{a_0}{\sqrt{\lambda}}\frac{\boldsymbol{R}}{R}. \tag{19}$$

Taking into account that during deformation the subchain length is $R = l = \lambda l_0 = \lambda a_0$, we get from Eq. (19)

$$\mathbf{F}_{\mathrm{LJ}}(\boldsymbol{R}) = \frac{3k_{\mathrm{B}}T}{a_0^2}k_{\mathrm{LJ}}(\lambda)\frac{1}{\lambda^{3/2}}\boldsymbol{R}. \tag{20}$$

Therefore, the interchain repulsive, excluded-volume interactions are accounting for in the model by introducing an extra term in the intrachain tension, due to the pressure which acts against the tube wall. Thus, the additional stress tensor can be written as

$$\begin{aligned}\boldsymbol{\tau}_{\mathrm{p}}^{\mathrm{INTER}} &= cZ < \boldsymbol{F}_{\mathrm{LJ}}\boldsymbol{R} > = cZ\frac{3k_{\mathrm{B}}T}{a_0^2}k_{\mathrm{LJ}}\frac{1}{\lambda^{3/2}}\langle\boldsymbol{RR}\rangle \\ &= cZ_0 3k_{\mathrm{B}}Tk_{\mathrm{LJ}}\frac{1}{\lambda^2}\frac{\langle\boldsymbol{RR}\rangle}{a_0^2},\end{aligned} \tag{21}$$

or

$$\boldsymbol{\tau}_{\mathrm{p}}^{\mathrm{INTER}} = Gk_{\mathrm{LJ}}(\lambda)\frac{1}{\lambda^2}(\boldsymbol{\sigma}-\boldsymbol{I}). \tag{22}$$

Hence, the total polymeric stress tensor that combines both the intrachain tension and the interchain interactions is written in the following form

$$\boldsymbol{\tau}_{\mathrm{p}} = \boldsymbol{\tau}_{\mathrm{p}}^{\mathrm{INTRA}} + \boldsymbol{\tau}_{\mathrm{p}}^{\mathrm{INTER}} = G\left[k_{\mathrm{s}}(\lambda)\frac{1}{\lambda} + k_{\mathrm{LJ}}(\lambda)\frac{1}{\lambda^2}\right](\boldsymbol{\sigma}-\boldsymbol{I}). \tag{23}$$

As is apparent from Eq. (23), the stress tensor results from traction in the axial direction (intrachain interactions) and interchain repulsive interactions (due to the pressure that the confined chain exerts on the tube wall) which is included as an extra term in the intrachain tension. Eq. (23) also accounts for the tube diameter variation, in terms of the stretch ratio, λ, through the relation, $a = a_0/\lambda$.

Finally, the expression for the tensor function, $\boldsymbol{f}$, given by Eq. (3) used in the constitutive equation, Eq. (1), has to be modified by using an effective spring coefficient that combines both k_{s} and k_{LJ}, i.e, $k_{\mathrm{eff}} = k_{\mathrm{LJ}} + k_{\mathrm{s}}$, instead of the sole spring coefficient k_{s}. Therefore, the effects of interchain, excluded-volume interactions are included in the dynamic equation, Eqs. (1) and (3), through the effective spring coefficient. The consequence of using an extra term in the intrachain tension on the rheology of linear entangled polymers is analyzed in the following section.

As an alternative to the LJ potential, we have also employed a purely repulsive potential for which the spring coefficient of the "virtual spring", k_{LJ}, is replaced by an exponential coefficient, k_{exp}, given by

$$k_{\mathrm{exp}}(\lambda) = \exp\left[3\alpha\left(\lambda^2 - 1\right)\right]. \tag{24}$$

Table 1
Linear viscoelastic properties of the polystyrene melts PS200k and PS390k at 130 °C [8]

Polymer	η_0 (MPa s)	τ_{d} (s)	τ_{R} (s)	Z
PS200k	84	1040	23	15
PS390k	755	11300	130	29

With the proper choice of the parameter α, this force law coefficient is shown to predict the proper power law dependence, as discussed in the next section.

4. Uniaxial extensional flow

In order to understand the behavior of the Rolie-Poly model with the direct interchain excluded-volume interactions, we performed steady steady-state uniaxial extensional flow simulations, and compared the predictions with the experimental results. The fluid parameters are those of the polystyrene polymer melts (PS200k and PS390k) studied experimentally by Bach et al. [8]. These are given in Table 1. The two time scales, τ_{d} and τ_{R}, are related by $\tau_{\mathrm{d}} = 3Z\tau_{\mathrm{R}}$ [20]. The other fluid parameters used in the model are: $\beta = 0.1$, and $\delta = -0.5$. The maximum stretch ratio is set to $\lambda_{\mathrm{max}} = 4.5$, in the nonlinear spring coefficient, Eq. (5). It has been shown that this value of λ_{max} is appropriate for PS melts [10]. Let us now analyze, in Fig. 1, the effect of interchain, repulsive excluded-volume interactions, by means of the LJ potential and a purely repulsive exponential potential with various parameter α. Fig. 1 shows the extensional viscosity, η_{el}, as a function of the reptation time-based Deborah number, $De_{\mathrm{d}} = \dot{\varepsilon}\tau_{\mathrm{d}}$. The parameters used are those of the polystyrene PS200k. Overall, the model predicts a monotonic decrease in extensional viscosity without showing any sign of an upturn well beyond, $\dot{\varepsilon}\tau_{\mathrm{R}} = 1$. This behavior is only due to the interchain excluded-volume interactions between polymer chains. The initial drop from the Newtonian value is due to tube orientation in the elongation direction. We also note that the slope of the extensional viscosity η_{el} depends on the interaction potential field used to characterize the interactions between polymer chains and seems to slightly decrease at very high De_{d}. With a proper choice of the parameter α, the exponential repulsive potential gives good qualitative and quantitative predictions, as highlighted in

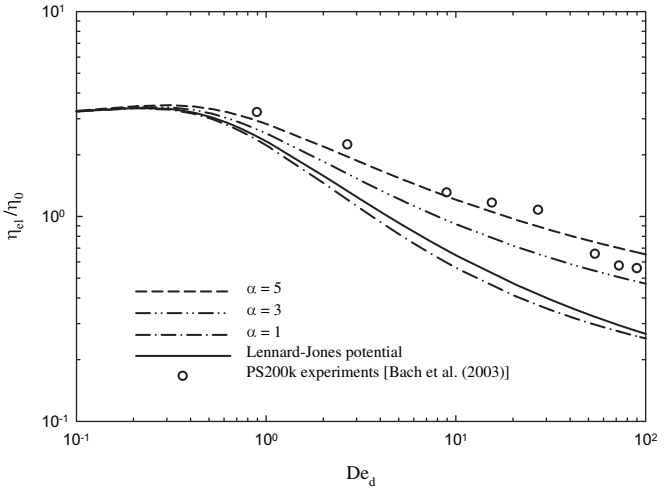

Fig. 1. Steady-state extensional viscosity normalized with zero shear viscosity for PS200k as a function of the reptation time-based Deborah number, $De_{\mathrm{d}} = \dot{\varepsilon}\tau_{\mathrm{d}}$: effects of interchain excluded-volume interactions using different interaction potentials. The open circles represent the experimental data of Bach et al. [8].

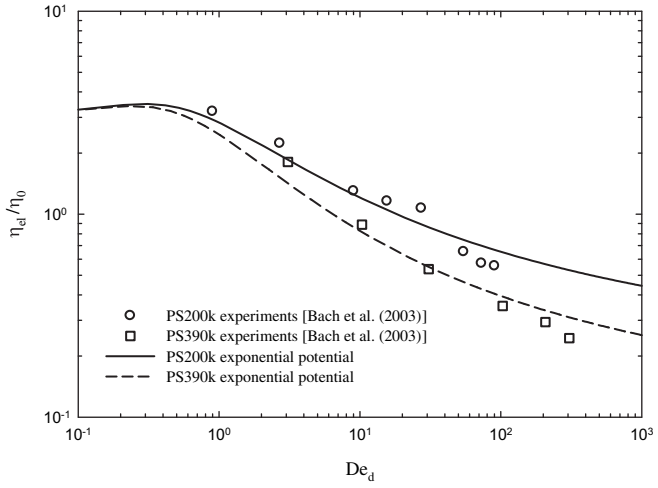

Fig. 2. Steady-state extensional viscosity normalized with zero shear viscosity for PS200k and PS390k as a function of the reptation time-based Deborah number, $De_d = \dot{\varepsilon}\tau_d$, compared to the experimental data of Bach et al. [8]: effects of interchain excluded-volume interactions, with $\alpha = 5$.

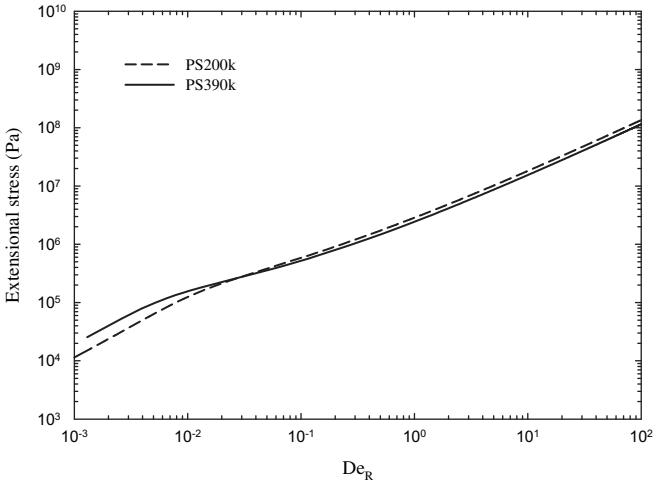

Fig. 4. Steady-state extensional stress for PS200k and PS390k as a function of the Rouse time-based Deborah number, $De_R = \dot{\varepsilon}\tau_R$: effects of interchain excluded-volume interactions, with $\alpha = 5$.

Fig. 1. The major feature of these results is the dependence of the slope of the extensional viscosity on the strength of the repulsive potential.

Now we perform a quantitative comparison with the experimental data of Bach et al. [8], in uniaxial extensional flow. The steady steady-state curves of the extensional viscosity as a function of the reptation time-based Deborah number De_d, for PS200k and PS390k are shown in Figs. 2 and 3. The predicted extensional viscosity curves decrease monotonically with the strain rate without any sign of upturn in the vicinity of $\dot{\varepsilon}\tau_R \approx 1$. The effect of interchain excluded-volume interactions is further highlighted in Fig. 3, which also includes the extensional viscosity prediction in the absence of excluded-volume interactions. We observe that, the extension thinning behavior becomes more pronounced in the absence of interchain excluded-volume interactions. Moreover, unlike the experimental data, we observe an upturn of η_{el} at $\dot{\varepsilon}\tau_R > 1$ (which corresponds to $De_d > 30$) when excluded-volume interactions are not included. In this case, predictions become sensitive to the value of the maximum stretch ratio and, the extensional viscosity ultimately saturates when the chains become fully stretched. This trend of the extensional viscosity, η_{el}, was confirmed experimentally for monodisperse entangled PS solutions only [20], and can be explained as follows. The initial drop from the Newtonian value is due to tube orientation in the elongation direction that, in the absence of chain stretch, would saturate the extensional stress [3]. Hence, in the absence of interchain excluded-volume interactions, the extensional viscosity decreases, approaching the slope −1 in the log plot (dashed-dot-dot line in Fig. 3). However, at higher elongation rates and in the absence of interchain excluded-volume interactions, excessive chain stretch makes the viscosity increase. Finally, finite extensibility brings the viscosity to a saturation value [3] (dashed-dot-dot line in Fig. 3). Conversely, according to the model developed here that incorporates interchain excluded-volume interactions, whenever a subchain changes its length, the diameter of the tube which surrounds the subchain changes, so as to keep the volume of the tube segment constant (incompressibility assumption). As mentioned previously, in such

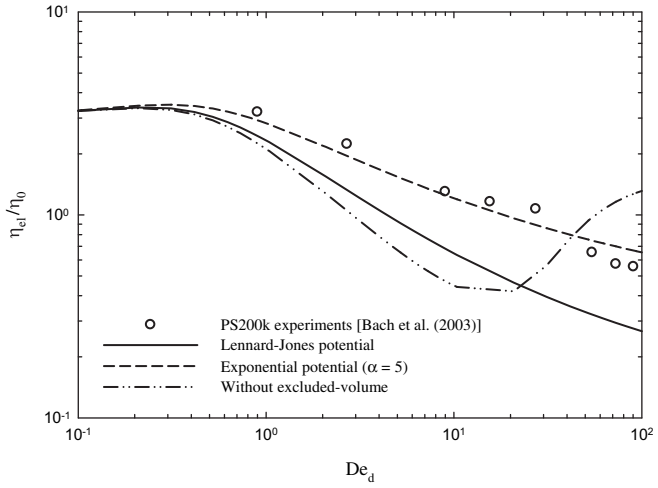

Fig. 3. Steady-state extensional viscosity normalized with zero shear viscosity for PS200k as a function of the reptation time-based Deborah number, $De_d = \dot{\varepsilon}\tau_d$, compared to the experimental data of Bach et al. [8]: effects of interchain excluded-volume interactions using different interaction potentials.

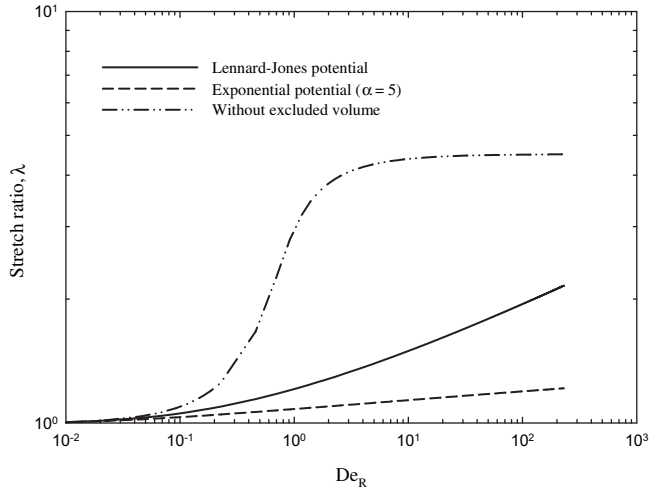

Fig. 5. Steady-state stretch ratio, λ, for PS200k as a function of the Rouse time-based Deborah number, $De_R = \dot{\varepsilon}\tau_R$: effects of interchain excluded-volume interactions using different interaction potentials.

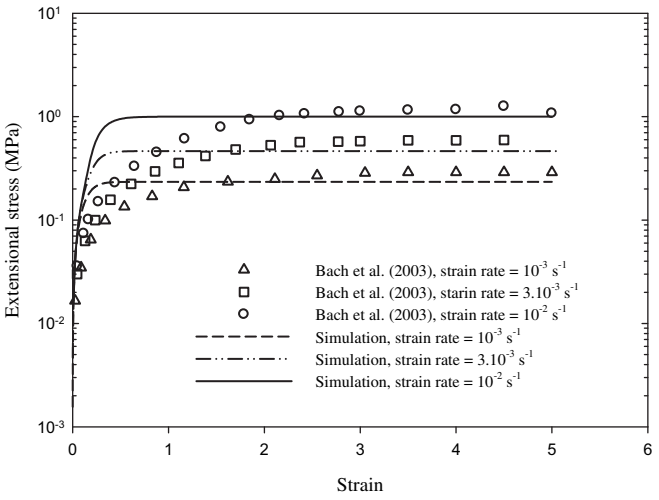

Fig. 6. Transient extensional stress response for PS200k at various strain rates as a function of the Hencky strain, compared to the experimental data of Bach et al. [8]. Predictions are obtained using the exponential potential with $\alpha = 5$.

a situation, due to the shrinkage of the tube diameter, the primitive chain experiences topological constraints at an average distance, $a = a_0/\lambda$, smaller than the equilibrium distance, a_0. The interaction between the test chain and the topological constraints generates a large repulsive force which, in turn, prevents excessive chain stretching. Hence, when interchain excluded-volume interactions are accounted for, the extensional viscosity decreases, approaching the slope -0.5 in the log plot that depends on the strength of the repulsive potential. Furthermore, when a purely repulsive exponential potential is used, a reasonable quantitative agreement between predictions and experimental data for entangled PS melts is obtained as shown in Figs. 1–3. This potential contains only one adjustable parameter, α. We would like to point out that, although the extensional viscosity predicted by using the LJ potential did not show any sign of an upturn well beyond $\dot{\varepsilon}\tau_R = 1$, it fails to predict the correct slope of the extensional viscosity. As an alternative to Fig. 2, we show in Fig. 4 the predicted steady-state extensional stress for the two polystyrene melts as a function of the Rouse time-based Deborah number, $De_R = \dot{\varepsilon}\tau_R$. In the stretching regime for which, $\dot{\varepsilon}\tau_R > 1$, the steady-state extensional stress predictions for PS200k and 390k give almost the same results and fall onto a unique curve.

In Fig. 5, we display the steady-state stretch ratio for PS200k as a function of the Rouse time-based Deborah number, $De_R = \dot{\varepsilon}\tau_R$. For comparison, Fig. 5 also includes results without excluded-volume interactions in the model. In the stretching regime $(\dot{\varepsilon}\tau_R > 1)$, the steady-state stretch prediction without exclude-volume interactions becomes sensitive to the value of the maximum stretch ratio and, an overly rapid rise of the chain stretch toward its maximum extensibility is observed. When excluded-volume interactions are include, the model predicts a gradual increase of the chain stretch with the strain rate, without reaching its full extension, at least in the range of strain rate investigated. Therefore, the rapid rise of the chain stretch when excluded-volume interactions are not included, clearly shows that classical tube-based models with a constant tube diameter, overestimate the deformation of the chains.

Finally, in Fig. 6 we compare the prediction of the transient extensional stress as function of Hencky strain, in start-up of uniaxial extensional flow to the experimental data for PS200k. While the steady steady-state predictions are in agreement with the experimental data, the model predicts faster growth of the extensional stress at low strains than the one measured experimentally, due to the strength of the repulsive potential.

5. Conclusions

We have presented an extension of the Rouse-CCR tube model for linear entangled polymers (Rolie-Poly constitutive equation), which incorporates interchain repulsive excluded-volume interactions to interpret extensional viscosity data of narrow molecular weight distribution polystyrene melts in extensional flow. The rheological behavior of the model was favorably compared with various results already published in the literature for entangled monodisperse polystyrene melts [8] and the regime of extensional thinning observed by Bach et al. [8] was correctly predicted. This regime extends well beyond $\dot{\varepsilon}\tau_R > 1$, as noted by Luap et al. [10]. Particularly, the predicted degree of chain stretching suggests that, in the regime of strain rate investigated here and in Bach et al., the chains did not reach their full extension.

References

[1] Doi M, Edwards SF. The theory of polymer dynamics. New-York: Clarendon; 1986.
[2] Mead DW, Larson RG, Doi M. Macromolecules 1998;31:7895.
[3] Marrucci G, Iannirubertо G. Philos Trans R Soc Lond A 2003;361:677.
[4] Moore JD, Cui ST, Cochran HD, Cummings PT. Phys Rev E 1999;60:6956.
[5] Padding JT, Briels WJ. J Chem Phys 2001;118:10276.
[6] Marrucci G, Iannirubertо G. Macromolecules 2004;37:3934.
[7] Marrucci G, Iannirubertо G. J Non-Newtonian Fluid Mech 2005;128:42.
[8] Bach A, Almdal K, Ramsmussen HK, Hassager O. Macromolecules 2003;36:5174.
[9] Graham RS, Likhtman AE, McLeish TCB, Milner ST. J Rheol 2003;47:1171.
[10] Luap C, Müller C, Schweizer T, Venerus DC. Rheol Acta 2005;45:83.
[11] Iannirubertо G, Marrucci G. J Non-Newtonian Fluid Mech 200;102:383.
[12] Likhtman AE, Graham RS. J Non-Newtonian Fluid Mech 2003;114:1.
[13] Wagner MH, Rubio P, Bastian H. J Rheol 2001;45:1387.
[14] Iannirubertо G, Marrucci G. J Non-Newtonian Fluid Mech 1998;79:225.
[15] Marrucci G. J Non-Newtonian Fluid Mech 1996;62:279.
[16] Kabanemi KK, Hétu JF. J Non-Newtonian Fluid Mech 2009;160:113.
[17] Pattamaprom C, Driscroll JJ, Larson RG. Macromol Symp;158:1.
[18] Marrucci G, de Cindio B. Rheol Acta 1980;19:68.
[19] Fetsko SW, Cummings PT. Int J Thermophys 1994;15:1085.
[20] Ye X, Larson RG, Pattamaprom C, Sridhar T. J Rheol 2003;47:443.